IEEE Access
Multidisciplinary | Rapid Review | Open Access Journal

Received 19 June 2025, accepted 29 June 2025, date of publication 11 July 2025, date of current version 31 July 2025.

Digital Object Identifier 10.1109/ACCESS.2025.3588443

RESEARCH ARTICLE

Multi-Objective Optimization of Machine Learning-Based Nonlinear Equalizers for Digital Coherent Optical Interconnects

LUCAS C. DANTAS[1], HILDO GUILLARDI JÚNIOR[1], PLINIO DESTER[1], RAFAEL A. PENCHEL[1], (Senior Member, IEEE), JOSÉ AUGUSTO DE OLIVEIRA[1], MARCELO L. F. ABBADE[1], LEANDRA I. ABREU[1], JINLONG WEI[2], (Senior Member, IEEE), AND IVAN ALDAYA[1], (Member, IEEE)

[1]Electronic and Telecommunications Engineering Department, São Paulo State University, São João da Boa Vista, São Paulo 01049-010, Brazil
[2]Pengcheng Laboratory, Shenzhen 518055, China

Corresponding author: Ivan Aldaya (ivan.a.aldaya@ieee.org)

This work was supported in part by São Paulo Research Foundation (FAPESP) under Project 2024/01712-9, in part by the National Council for Scientific and Technological Development (CNPq) and Financiadora de Estudos e Projetos (FINEP) under Project 313378/2021-5 and Project 0527/18, and in part by the Coordination for the Improvement of high Education Personnel (CAPES).

ABSTRACT The growing demand for high-capacity optical networks has driven the advancement of digital coherent optical communication systems, which rely on sophisticated signal processing to mitigate transmission impairments, including nonlinear fiber distortions. Traditional nonlinear compensation techniques, such as the Inverse Volterra Series Transfer Function (IVSTF) and Digital Back Propagation (DBP), are computationally expensive and require oversampling. Machine learning-based equalizers offer reduced complexity and improved adaptability. However, for dispersion-uncompensated systems with a high bandwidth-reach product, the computational complexity increases, becoming a significant concern. This work presents a multi-objective optimization approach for nonlinear equalization, balancing performance and computational cost. A sequentialized multilayer perceptron (MLP)-based nonlinear equalizer is applied to a 16-QAM digital coherent optical system over a 150 km uncompensated link at 112 Gbps. Various hyperparameter configurations, tap and neuron counts, are evaluated to identify optimal trade-offs. A Pareto front analysis quantifies the complexity-performance trade-off, providing insights into selecting an optimal equalizer configuration based on system constraints.

INDEX TERMS Digital coherent optical communication systems, nonlinear distortion, equalizer.

I. INTRODUCTION

The remarkable advancements in telecommunications over recent decades have been driven by the evolution of optical networks, developed to accommodate the ever-growing demand for higher data transmission capacities [1], [2]. A key breakthrough in this field was the introduction of digital coherent optical communication systems [3], which revolutionized data transmission by enabling advanced modulation formats that leverage both phase and polarization diversity. Additionally, these systems have made it possible to digitally compensate for transmission impairments [4]. By utilizing high-speed digital signal processors (DSPs), digital coherent systems effectively mitigate issues such as chromatic dispersion, polarization-mode dispersion, phase noise, and frequency mismatch. Consequently, their performance is primarily limited by the combined effects of additive noise and nonlinear distortions [5]. While noise originating from optical amplifiers or receiver photodetectors is inherently stochastic and exhibits a short coherence time, nonlinear distortions induced by the fiber are deterministic and, in principle, more manageable. In digital coherent communication systems, where narrow-linewidth frequency components are not present, the dominant nonlinear effect is the fiber's Kerr effect [6], [7], [8], [9]. This effect exhibits a complex interaction with linear phenomena such

The associate editor coordinating the review of this manuscript and approving it for publication was San-Liang Lee.

© 2025 The Authors. This work is licensed under a Creative Commons Attribution 4.0 License.
For more information, see https://creativecommons.org/licenses/by/4.0/

as attenuation and chromatic dispersion, posing significant challenges to effective compensation [10].

In recent years, different approaches have been explored to mitigate fiber-induced nonlinear distortion. Optical methods, such as mid-span compensation, exploit system symmetry to simultaneously counteract linear and nonlinear distortions [11], [12]. However, these techniques require a careful design of the link, making their commercial adoption challenging. In contrast, electronic techniques exploit the flexibility of digital processing, allowing more adaptable solutions. The first electronic compensation techniques relied on model inversion. The Inverse Volterra Series Transfer Function (IVSTF) [13] and Digital Back Propagation (DBP) [14] were extensively studied, but they present two significant challenges: they are computationally demanding and require oversampling of the received signal to capture out-of-band frequency components generated by nonlinear interactions. To alleviate these limitations, machine learning-based techniques have been explored as an alternative. These approaches generally offer lower computational complexity compared to traditional model inversion methods and can operate directly on the sampled distorted symbols, eliminating the need for oversampled reception [15].

The wide range of machine learning-based nonlinear compensation techniques can be categorized according to different criteria [16]. One possible classification depends on whether the technique employs only the information of the symbol to be corrected or also exploits the information of adjacent symbols. In other words, it depends on whether the method has memory or not. For systems with low baud rate-range products or with in-line chromatic dispersion compensation, the self-phase modulation of the symbol is dominant, and memoryless techniques may exhibit reasonable performance. Among the different memoryless techniques, we can mention clustering algorithms [17], [18], [19], supervised classification [20], [21], [22], and supervised regression [23], [24]. However, for uncompensated high baud rate-range product systems, the nonlinear distortion caused by adjacent symbols becomes significant. There are three main approaches to tackle multi-symbol nonlinear distortion: sequentialized multi-layer perceptrons (MLPs) [25], [26], [27], convolutional neural networks (CNNs) [28], [29], [30], and recurrent neural networks (RNNs) [31], [32], [33].

In MLPs, CNNs, and RNNs, the mitigation capacity is improved at the cost of a significant increase in computational complexity [34]. Therefore, reducing computational cost has become an increasing concern [26], [35], [36], [37]. Nevertheless, power consumption is usually addressed sequentially. That is, the hyperparameters are first tuned, and then the computational complexity of the best-found configuration is computed. The main contribution of this work is that instead of calculating the complexity of only the best configuration, we compute the complexity of various configurations, allowing us to identify suboptimal configurations that offer lower computational costs while maintaining reasonable mitigation capabilities. In other words, we perform a multi-objective optimization of the equalizer. To evaluate the proposed optimization algorithm, we applied it to a dual-polarization (DP) 16-ary quadrature amplitude modulation (16-QAM) digital coherent optical interconnect with a 150 km uncompensated link operating at 112 Gbps. This bitrate was chosen because it leads to moderate nonlinear inter-symbol interference (ISI), which is desirable for better demonstrating the operation of the optimization technique. A lower bitrate would not result in significant ISI, whereas a higher baud rate would make an extensive search in the hyperparameter space more challenging. Although this configuration does not meet the specifications of 400ZR, it may be suitable for other heterogeneous applications, such as 5G edge communications [38]. Numerical results reveal that the chosen equalizer exhibits excellent granularity in the performance-complexity trade-off. The rest of this article is organized as follows: Section II describes the simulation setup and the employed equalizer. Results are presented in Section III. The extension of the proposed optimization method to compare different equalizer configurations or to evaluate its performance against other nonlinear compensation techniques is discussed in Section IV. Finally, Section V concludes the paper.

II. SIMULATION SETUP AND NONLINEAR EQUALIZER

Figure 1(a) illustrates the block diagram of the simulation setup designed to assess the performance of the nonlinear equalizer. The simulations were conducted in a VPI TransmissionMaker Python co-simulation environment, where signal generation, transmission, reception, and linear effect compensation were implemented in VPI TransmissionMaker, while nonlinear equalization, signal detection, and bit error ratio (BER) estimation were performed in Python.

A. SIMULATION SETUP

At the transmitter, two independent pseudorandom bit sequences (PRBSs) of length 2^{20} (1,048,576) were generated and mapped onto a complex base-band 16-QAM constellation. The in-phase and quadrature components were oversampled with a factor of 4 and filtered using raised-cosine Nyquist filters with a roll-off factor of 0.2 (which was selected following the suggestion of [39]). To emulate digital-to-analog (DAC) conversion, the number of samples per symbol was increased to 32. The signals were scaled to minimize the signal clipping and the nonlinear distortion caused by the optical modulators. The resulting electrical signals had a bandwidth of 8.4 GHz. The processed in-phase and quadrature components were then used to drive dual-parallel Mach-Zehnder modulators (DP-MZMs) with an insertion loss of 10 dB. These MZMs modulated each polarization of the optical wave with the corresponding PRBS data. The optical carriers fed into the two DP-MZMs were derived by splitting the orthogonal polarizations at the output of a continuous-wave (CW) laser diode (LD) with a 100-kHz

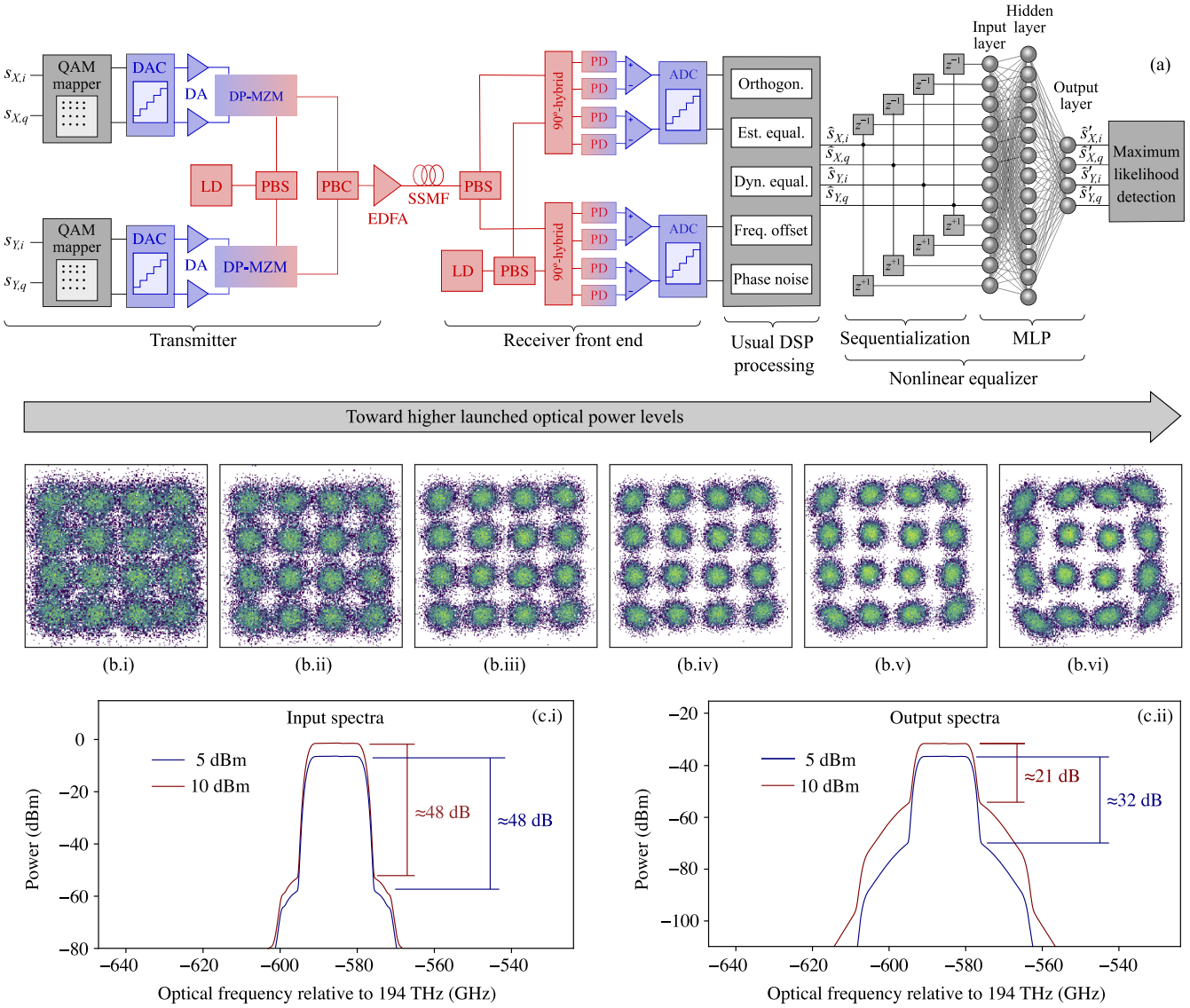

FIGURE 1. (a) Simulation setup block diagram. DAC: digital-to-analog converter, DA: driving amplifier, LD: laser diode, PBS: polarization beam splitter, DP-MZM: dual-parallel Mach-Zehnder modulator, PBC: polarization beam combiner, EDFA: erbium-doped fiber amplifier, SSMF: standard single-mode fiber, PD: photodetector, and ADC: analog-to-digital converter. $z^{\pm 1}$: one-symbol positive-negative offset. (b) Received constellations for launched optical power levels of b.i 1, b.ii 3, b.iii 5, b.iv 7, b.v 9, and b.vi 11 dBm. (c) The input and output spectra for 5 and 10 dBm launched optical power are presented in c.i and c.ii, respectively.

linewidth, an output power of 14 dBm, and a nominal emission wavelength of 1,550 nm. The modulated optical signals, corresponding to the two orthogonal polarizations, were subsequently combined using a polarization beam combiner (PBC). Finally, an erbium-doped fiber amplifier (EDFA) was employed to adjust the launched optical power at the transmission link input, varying between 0 and 15 dBm.

The dual-polarization 16-QAM signal was transmitted over a single span of standard single-mode fiber (SSMF) with a length of 150 km. The SSMF was simulated employing an adapted-step vectorial Split Step Fourier Method (SSFM) considering a dispersion parameter $D = 16$ ps/(nm·km), a dispersion slope of $S = 0.08$ ps/(nm^2· km), a polarization mode dispersion (PMD) parameter of $D_{PMD} = 0.01$ ps/$\sqrt{\text{km}}$, and an attenuation coefficient of $\alpha = 0.2$ dB/km. The modal effective area was set to $A_{eff} = 80\ \mu$ m^2 and the nonlinear Kerr-induced coefficient was $\gamma = 0.26\mu$ m^2/GW.

At the receiver side, the incoming signal was separated into its two orthogonal polarization components using a polarization beam splitter (PBS). Each component was then combined with a CW laser using a 90°-hybrid network with a 6 dB insertion loss, a phase imbalance of 10°, and a transmission loss difference of 1 dB. The outputs of the 90°-hybrid networks were detected by balanced photodetectors (PDs) with a responsitivity of 0.7 A/W and a thermal noise current density of 21 pA/$\sqrt{\text{Hz}}$. The photodetected signals were then differentially amplified. Following amplification, the four signals representing the in-phase and quadrature components of both polarizations were downsampled to two samples per symbol, simulating the operation of an analog-to-digital

converter (ADC). In order to consider a realistic ADC, simulations contemplated a clock jitter of 50 MHz and 8-bit quantization.

The digitized signals were processed in the DSP following a conventional block sequence [40]. First, the in-phase and quadrature components of each polarization were orthogonalized using the Gram-Schmidt method, which partially mitigates the phase imbalance of the 90°-hybrid and polarization-dependent loss. These components were then converted into a complex stream of samples and segmented for frequency-domain chromatic dispersion (CD) compensation. Next, dynamic multiple-input multiple-output (MIMO) equalization was performed using the multi-modulus algorithm (MMA). This dynamic equalizer had a two-fold purpose: on one hand, it compensated for the dynamic variation of PMD, the rotation of the state of polarization, and time-dependent polarization-dependent loss; on the other hand, it compensated for residual chromatic dispersion caused by deviations in the fiber's dispersion parameter from its nominal value. After equalization, the signals were synchronized and resampled using a clock-recovery algorithm based also on the MMA, achieving a single sample per symbol. The final stages included frequency offset correction and phase error compensation. Frequency offset was corrected by identifying the maximum peak of the periodogram and applying a linear phase shift, while phase error was mitigated using the widely adopted blind phase search algorithm operating on blocks of 5 symbols.

To qualitatively illustrate the combined effects of additive noise and nonlinearities as a function of launched optical power, Fig. 1(b) shows the received constellations at six distinct optical power levels (1, 3, 5, 7, 9, and 11 dBm). As the launched optical power increases, the scattering of points around the ideal symbol positions decreases, indicating a reduced relative contribution of additive noise. However, the constellation clusters experience nonlinear rotation, resulting in significant signal degradation. This effect is more pronounced for symbols at the periphery of the constellation, where higher power levels intensify the distortion. Nevertheless, the nonlinear distortion is not limited to the aforementioned phase rotation; it also contributes to point scattering in the constellation plane, which can be mistaken for additive noise. However, this point scattering is essentially deterministic and, consequently, can be partially mitigated by the nonlinear compensator. Nonlinear effects can also be observed in the frequency domain. To illustrate this, in Fig. 1(c)i and ii, we present the input and output spectra for two launched optical power levels. As can be seen, for a launched optical power of 5 dBm, the spectral widening is significantly lower than for 10 dBm, indicating that nonlinear effects are indeed present.

B. EQUALIZER IMPLEMENTATION AND TRAINING

To test the proposed optimization method, we decided to use a well-established machine-learning-based equalizer architecture, known as the sequentialized deep neural network [41]. Due to its training efficiency and intuitive interpretation, this equalizer has been employed in a broad variety of optical communication systems, including m-ary pulse amplitude modulation (PAM) systems based on directly modulated lasers [42] and digital coherent orthogonal frequency division multiplexing systems [43]. This equalizer architecture has also been applied to single-carrier coherent systems [25], [27], [44]. As shown in Fig. 1, this equalizer consists of two stages. The first stage, known as the sequentialization stage, extracts the in-phase and quadrature components of both the X and Y polarizations of successive symbols using positive and negative delay taps. It is important to note that at the output of the DSP processing, we used a time framework centered on the symbol of interest, following the approach proposed in [10]. This allows access to future adjacent symbols without violating the principle of causality. Given the symmetry around the symbol of interest, we use three taps to compensate for the influence of immediately adjacent symbols (a tap represents a time delay of the four components of the symbol): the preceding symbol, the symbol of interest, and the following symbol. For compensation involving two adjacent symbols, we employ five taps: two preceding symbols, the symbol of interest, and two following symbols. This procedure can be extended to an arbitrary number of symbols. For our particular case, we considered up to 7 adjacent symbols, that is, 15 taps.

Once the in-phase and quadrature components of the X and Y polarizations of successive symbols are grouped, the signals are processed using a multilayer perceptron (MLP). The MLP consists of an input layer with $4N_{\text{Taps}}$ neurons, a hidden layer with N_{neurons} neurons, and an output layer with four neurons. Preliminary simulations indicated that these are the two hyper-parameters that dominate the performance and complexity of the MLP architecture, while other hyper-parameters, such as the batch size, the configuration of the optimization engine, and the activation function, do not have a significant impact. In view of that, although complex activation functions such as the hyperbolic tangent and logistic regression can be implemented using look-up tables, we opted for ReLU to further reduce the latency and minimize the approximation error. The 70% of the simulated data were used for training, while the remaining 30% were used for testing the model. The model was trained using the well-known Adam optimizer, configured with $\beta_1 = 0.9$, $\beta_2 = 0.999$, and $\epsilon = 10^{-8}$. The batch size was set to 200 samples. To mitigate the effect of convergence to local minima, 20 runs were performed over blocks of 20,000 symbols for each configuration. We evaluated configurations considering N_{Taps} ranging from 1 to 15 (in intervals of 2) and N_{Neurons} spanning from 10 to 250 (in intervals of 10). Therefore, the total number of evaluated configurations is 200. These ranges of N_{Taps} and N_{Neurons} allow us to build the Pareto front for the specific system configuration and equalizer architecture. Nevertheless, these ranges may be adjusted for different system configurations.

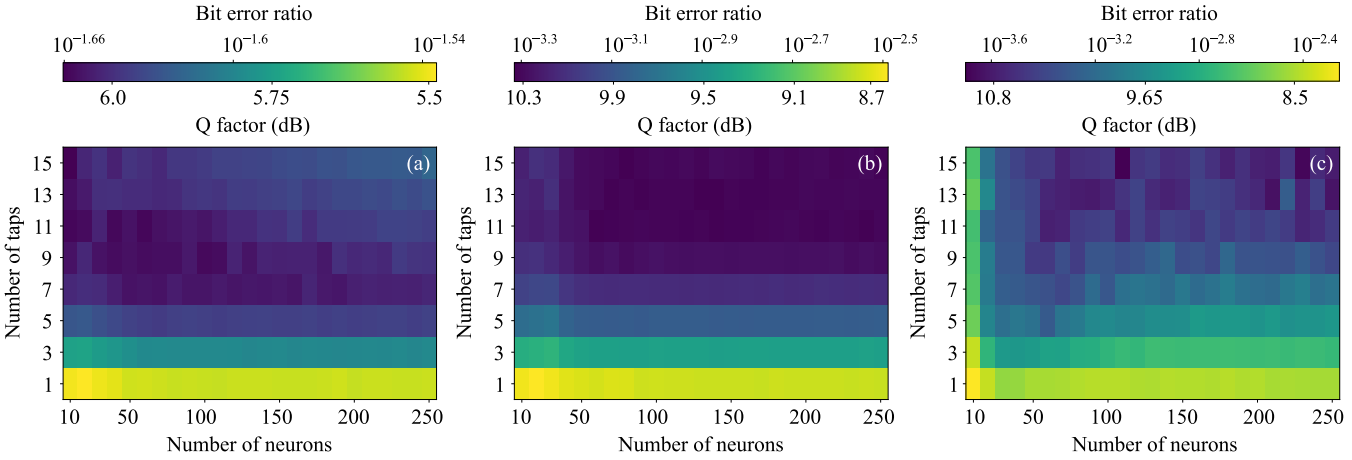

FIGURE 2. BER in terms of the number of taps and neurons in the hidden layer for (a) 1 dBm, (b) 6 dBm, and (c) 11 dBm. Each rectangle corresponds to one of the evaluated configurations.

C. BER ESTIMATION

The estimation of BER deserves special attention when dealing with nonlinearly distorted constellations. In particular, if self-phase modulation (SPM) is significant, the blind EVM method, widely used for BER estimation in noise-limited systems, leads to substantial BER underestimation. Therefore, it is necessary to estimate the BER through direct error counting. This method, however, has a minimum BER estimation threshold, which corresponds to the inverse of the number of transmitted bits. In our case, we process blocks of 20,000 symbols (160,000 bits), from which 30% (6,000 symbols, 48,000 bits) are used for training. Consequently, the minimum detectable BER is 10^{-5}, which is nearly an order of magnitude lower than the minimum obtained BER. Additionally, in the context of nonlinear equalization analysis, the equivalent Q-factor is often employed as an alternative metric to BER. The equivalent Q-factor is related to the BER through [45]:

$$Q_{\text{eq}} = \sqrt{2}\,\text{erfc}^{-1}(2\,\text{BER}), \tag{1}$$

where $\text{erfc}^{-1}(\cdot)$ denotes the inverse complementary error function. Thus, the variation of the equivalent Q-factor is particularly useful for quantifying signal quality improvement and is typically expressed as:

$$\Delta Q_{\text{eq}} = 20\log_{10}\left(\frac{Q_{eq}}{Q'_{\text{eq}}}\right)\,[\text{dB}], \tag{2}$$

being Q_{eq} the Q-factor of the signal when the equalizer is employed and Q'_{eq} a reference Q factor corresponding to the received signal in the absence of nonlinear equalization.

III. RESULTS

In this section, we first analyze the performance of the considered nonlinear equalizer and discuss the hyperparameter tuning. Next, we quantify the equalizer's complexity in terms of the hyperparameters. Finally, we present the obtained BER as a function of complexity for the different evaluated configurations.

A. PERFORMANCE ANALYSIS

All 200 combinations were evaluated for launched optical power ranging from 1 to 11 dBm. To present the results concisely and avoid excessively large images, Fig. 2 illustrates the BER as a function of the number of taps and the number of neurons in the hidden layer for three representative launched optical power levels: (a) low power, 1 dBm, (b) medium power, 6 dBm, and (c) high power, 11 dBm.

The first key observation is the difference in scale across the three subfigures. For 1 dBm, the BER ranges from $10^{-1.66}$ ($2.2 \cdot 10^{-2}$) to $10^{-1.53}$ ($2.9 \cdot 10^{-2}$), representing a Q-factor range of 0.5 dB. For 6 dBm, the variation is from $10^{-3.32}$ ($4.8 \cdot 10^{-3}$) to $10^{-2.48}$ ($3.2 \cdot 10^{-3}$), a Q-factor difference of 1.62 dB. Finally, for 11 dBm, the obtained BER ranges from $10^{-3.70}$ ($2.0 \cdot 10^{-4}$) to $10^{-2.26}$ ($5.5 \cdot 10^{-3}$), which corresponds to a Q-factor variation of 2.87 dB. This indicates that at low power levels, where nonlinear effects are minimal, the sensitivity of performance to hyperparameter variations is weak, as the equalizer has limited effectiveness. In contrast, the BER range becomes significantly broader at medium and high power levels. This trend highlights the increasing role of the nonlinear equalizer as launched power rises, making its hyperparameter selection more impactful.

For the purpose of equalizer optimization, medium and high power levels are of particular interest, as the nonlinear equalizer plays a crucial role in improving signal quality. In both cases, the number of taps has a greater influence on performance than the number of neurons. However, at high power levels, the number of neurons has a more pronounced effect compared to medium power levels because stronger nonlinear distortions at high power require a more complex equalizer to provide effective compensation. At medium power levels, a distinct region can be identified where BER variations remain low ($N_{\text{Taps}} \leq 11$ and $N_{\text{Neurons}} \leq 50$).

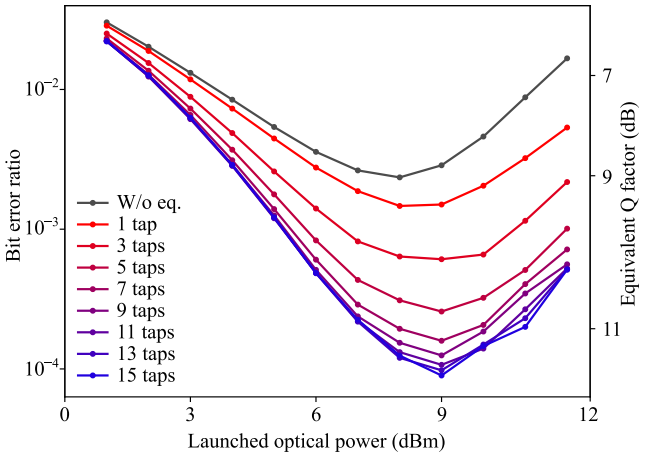

FIGURE 3. BER and equivalent Q-factor as a function of the launched optical power for different numbers of taps (number of processed symbols) considering 100 neurons. The BER curve in the absence of a nonlinear equalizer has been included as benchmark.

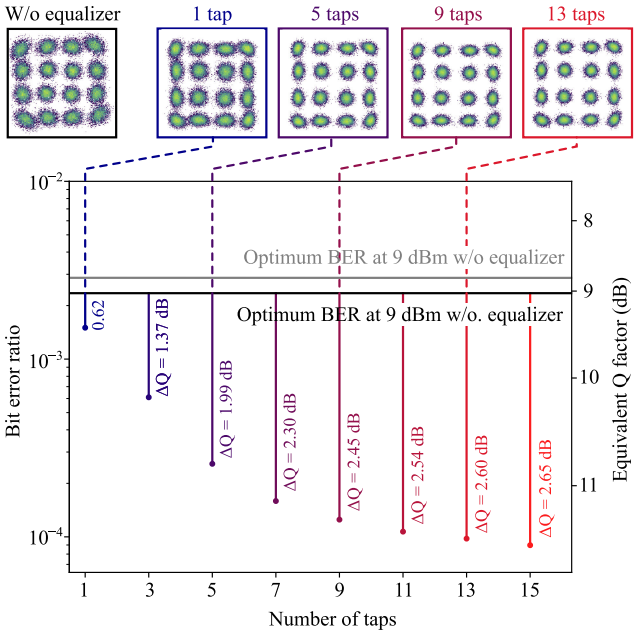

FIGURE 4. BER and Q-factor as a function of the number of taps for a launched optical power of 9 dBm. To qualitatively illustrate the performance improvement, the constellations without equalization and with 1-, 5-, 9-, and 13-tap equalizers are presented.

Within this region, increasing the equalizer's complexity yields minimal performance improvements. In other words, an equalizer with significantly lower computational complexity can be designed without substantially degrading performance, making it an optimal trade-off between efficiency and effectiveness.

In order to quantify the effect of tap numbers for different power levels, in Fig. 3 we present the BER and Q-factor as a function of the launched optical power for different values of this hyperparameter. The compensation capability is evident, reducing the optimum BER from $2.4 \cdot 10^{-3}$ to $8.9 \cdot 10^{-5}$, which is in agreement with the optimum launched optical power level reported in [46]. This reduction is particularly noticeable in the medium- and high-power regimes, where nonlinear effects are more pronounced. However, at elevated power levels ($\geq$ 11 dBm) and with a large number of processed symbols, the interaction among numerous interfering symbols leads to a more complex loss function, leading to training challenges and some performance variations. In addition, at such high power levels, the performance of the DSP modules responsible for compensating linear effects degrades, placing greater pressure on the nonlinear equalizer. Additionally, the shift of the optimum power from 8 to 9 dBm indicates that the equalizer is mitigating the nonlinear effects, thus reducing the relative impact of nonlinearities. Even if the largest BER reduction occurs at moderate and high launched optical power, it is also observed some BER reduction at low launched optical power levels, where fiber nonlinearities are weak. This improvement can be attributed to the equalizer compensating for residual nonlinear distortions introduced by the transmitter, which are introduced in Section II-A.

To analyze the effect of the number of processed symbols, Fig. 4 presents the BER as a function of this parameter for a launched optical power of 9 dBm. The number of neurons was set to 60. As observed, increasing the number of processed symbols reduces the BER, indicating that nonlinear intersymbol interference is being mitigated more effectively. We have included the BER values obtained in the absence of an equalizer for both 8 dBm and 9 dBm. The 8 dBm case is included as it corresponds to the best BER performance without equalization, while 9 dBm is considered since the equalizer's performance is evaluated at this power level. Additionally, we present the Q-factor improvement, which ranges from 0.62 dB for a single symbol to 2.65 dB for processing 15 symbols. This Q-factor improvement is calculated using the 8 dBm case without equalization as a benchmark. However, it is important to note that the improvement is even greater when compared to the 9 dBm case. As shown, BER improvement begins to saturate for symbol counts greater than 11, achieving a BER below 10^{-4}—a reduction of more than one order of magnitude, even when the input BER exceeds 10^{-3}. The impact of the equalizer, particularly the number of processed symbols, can be visually assessed in the presented constellations.

B. COMPLEXITY ANALYSIS

Since nonlinear effects in digital communication systems tend to exhibit long coherence times, training and hyperparameter tuning are expected to be performed infrequently. Actually, the model parameters for different channel conditions can be stored in memory and employed on-demand in combination with a channel condition assessment module. Therefore, in most cases, complexity analysis focuses on the prediction stage, assuming the model has already been optimized. The most common metric for assessing the complexity of an equalizer is the number of floating-point

operations (FLOPs) required to process a single symbol, which is a machine-independent metric. That is, for a given implementation platform, particularly field-programmable gate arrays (FPGAs) or application-specific integrated circuits (ASICs), the power consumption is proportional to the number of FLOPs to be performed. Generally speaking, ASICs tend to show higher power efficiency than FPGAs, but this comparison is highly dependent on the evolution of these platforms [47]. For the equalizer under analyis the number of FLOPs per symbol is:

$$N_{\text{op}} = (4N_{\text{Taps}} + 1)N_{\text{Neurons}} + 4(N_{\text{Neurons}} + 1). \quad (3)$$

In Fig. 5 we present the complexity as a function of the number of taps and neurons in the hidden layer. As observed, the complexity increases more gradually with the number of neurons compared to the increase in the number of taps. This can be explained by noting that increasing N_{sym} by a single unit has a greater impact due to its relatively low initial value, resulting in a larger relative increase. As we will see, this will have a significant impact when analyzing the complexity-performance trade-off.

Another important metric is the processing latency, which has two components. On one hand, the time required to receive the symbols to be processed, which is lower bounded by $N_{\text{Taps}} \cdot R_B$, where R_B is the system baud rate. On the other hand, the time required to process the symbols in the multi-layer perceptron, specifically the amount of sequential FLOPs required to process each symbol. Due to the structure of the equalizer, the operations in each neuron can be performed in parallel. Therefore, we can calculate that the number of sequential operations in a single-layer equalizer is:

$$N_{\text{seq}} = N_{\text{Taps}} + N_{\text{Neurons}}. \quad (4)$$

Once the number of sequential operations is determined, the actual processing time will depend on the adopted implementation platform. Even though a precise quantitative comparison is challenging, it is expected that, with current technologies, ASIC-based equalizers will outperform those relying on FPGAs [47]. Compared to the DSP modules responsible for compensating CD, PMD, and other nonlinear effects, the processing latency is expected to be much shorter. Therefore, in the following, we will focus on the performance-complexity trade-off.

C. COMBINED PERFORMANCE AND COMPLEXITY ANALYSIS

In Fig. 6 we present the BER when the nonlinear equalizer is employed, as a function of its complexity for different equalizer configurations. As expected, there is a trade-off between nonlinear compensation capability and the complexity of the equalizer. Specifically, achieving a lower BER requires a more complex equalizer. This represents a typical multi-objective optimization problem, where the two objective functions are mutually exclusive, resulting in a Pareto front. The Pareto front consists of the Pareto optimal

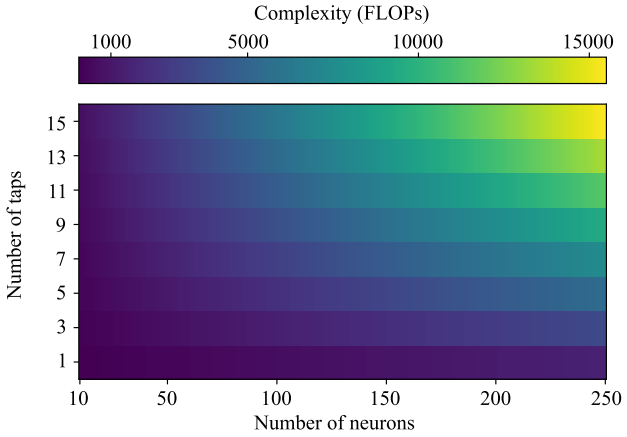

FIGURE 5. Complexity in terms of the number of taps and the number of neurons in the hidden layer. For each power level, the Pareto front is presented.

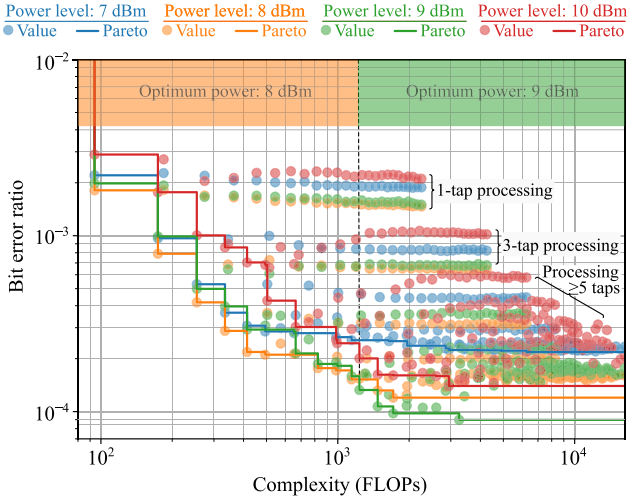

FIGURE 6. BER in terms of the complexity for the evaluated configurations considering launched optical power levels of 7, 8, 9, and 10 dBm.

solutions. In the context of multi-objective optimization, a Pareto optimal solution is a non-dominated solution, meaning that for a given value of one objective function, no other solution outperforms it in the other objective functions. In our case, a solution given by (C^*, BER^*) belongs to the Pareto front if, for all solutions satisfying $BER \leq BER^*$, the complexity of the solution is $C > C^*$. Due to the discrete nature of the model's hyperparameters, the Pareto front exhibits a step-like shape.

We performed this analysis for four launched optical power levels, namely 7, 8, 9, and 10 dBm. The results indicate that at 7 and 10 dBm, no dominant solution is found. For 8 and 9 dBm, on the other hand, different dominant solutions emerge. Comparing the Pareto fronts for the four power levels, we observe that for 7 and 10 dBm, all solutions are outperformed (in the Pareto sense) by those corresponding to 8 and 9 dBm. However, when comparing the Pareto fronts for the intermediate power levels (8 and 9 dBm), two distinct regions can be identified. For complexities

below approximately 1050 FLOPs (corresponding to BER values above 1.5×10^{-4}), better configurations are found at 8 dBm. Conversely, for complexities exceeding ≈1050 FLOPs, slightly better configurations are achieved with a launched optical power of 9 dBm.

The Pareto front in the BER-complexity design plane is a powerful tool as it provides valuable insight into the performance gains achieved by increasing the computational complexity of the equalizer. For instance, as observed in Fig. 6, increasing the computational complexity from 3×10^3 to 10^4 does not result in any performance improvement. Additionally, the Pareto front analysis enables engineers to fine-tune the model's complexity according to specific requirements while avoiding overdimensioning and unnecessary complexity. For instance, if the required FEC limit is 10^{-3}, the designer can set the launched optical power to 8 dBm and select a configuration with a complexity as low as 200 FLOPs. However, if a stricter BER requirement is imposed, such as 10^{-4}, a higher launched optical power of 9 dBm will be needed, along with a more complex configuration. This method was applied to a simple scenario where the Pareto front could be determined through an exhaustive search by sweeping the two main architectural hyperparameters. Nevertheless, the method can be extended to a larger number of hyperparameters as long as the two metrics (performance and computational cost) remain representative of the system.

IV. DISCUSSION

This section explores the broader applicability of the proposed multi-objective optimization approach, including its extension to alternative system configurations and its potential for enabling fair comparisons among different nonlinear compensation techniques. We also briefly address the challenges posed by high-dimensional scenarios and discuss strategies to mitigate them.

A. COMPARISON OF DIFFERENT CONFIGURATIONS

The proposed optimization framework can be extended to various system scenarios, such as longer links, higher baud rates, and multi-span or multi-channel configurations. In particular, for longer distances, exceeding the nonlinear effective length, increased power loss and photodetector noise reduce compensation effectiveness, causing a vertical shift in the Pareto front. Regarding higher baud rates, it will lead to an increased ISI, requiring more taps and leading to more complex equalizers and a diagonal shift of the Pareto front. A similar behavior is expected in multi-span systems, where accumulated dispersion exacerbates ISI. Optical amplifiers further amplify broadened signals, compounding the distortion. On the other hand, in multi-channel scenarios, outcomes depend on how interchannel interference is handled. If treated as noise, the case is analogous to longer links. If mitigated through joint channel processing, the configuration resembles the high-baud-rate case, requiring more taps and increased network complexity.

B. COMPARISON OF DIFFERENT TECHNIQUES

Comparing nonlinear compensation methods using a single performance metric can be misleading, as all electronic-based compensation techniques inherently involve trade-offs between computational complexity and performance. For example, in digital DBP, reducing the spatial step size enhances performance but significantly increases computational cost. Similarly, for equalizers based on the IVSTF, both complexity and compensation performance depend on parameters such as the Volterra order, oversampling factor, and block size [48]. The proposed optimization algorithm can be extended to support multi-criteria comparisons by analyzing the Pareto fronts of different techniques, thereby offering a more comprehensive view of the performance-complexity trade-off. Depending on system constraints, different techniques may be optimal at different points along this trade-off curve.

C. THE PARETO FRONT IN HIGH DIMENSIONAL SYSTEMS

In high bit-rate, multi-span, or multi-channel scenarios, the dimensionality of the equalizer increases due to intensified ISI. This raises two challenges: increased training complexity and a larger hyperparameter space. Exhaustive tuning becomes impractical, making efficient algorithms necessary. The Nondominated Sorting Genetic Algorithm II (NSGA-II) is particularly suitable for these conditions, as it enables effective estimation of the Pareto front with significantly fewer objective function evaluations [49].

V. CONCLUSION

In this work, we explored a multi-objective optimization approach for nonlinear equalization in digital coherent optical communication systems. We analyzed the performance-complexity trade-off of an MLP-based nonlinear equalizer applied to a 16-QAM system over a 150 km uncompensated fiber link operating at 112 Gbps. By systematically sweeping the two key structural hyperparameters, i.e. the number of taps and hidden layer neurons, we were able to find the Pareto front for different launched optical power levels. This study indicates that, from a multi-objective optimization perspective, there is no unique optimum launched optical power but may dependent on the system requirements. The Pareto front analysis provides a quantitative measurement of the trade-off between computational complexity and performance, enabling the selection of optimal equalizer configurations that balance mitigation capacity and efficiency. Future work can extend this approach to more complex optical networks, including multi-span links, where computational constraints become even more critical. Exploring advanced optimization techniques, such as evolutionary algorithms, may further refine the equalizer's efficiency.

REFERENCES

[1] M. Yücel and M. Açikgöz, "Optical communication infrastructure in new generation mobile networks," *Fiber Integr. Opt.*, vol. 42, no. 2, pp. 53–92, Mar. 2023.

[2] B. J. Puttnam, G. Rademacher, and R. S. Luís, "Space-division multiplexing for optical fiber communications," *Optica*, vol. 8, no. 9, pp. 1186–1203, 2021.
[3] G. P. Agrawal, *Fiber-Optic Communication Systems*. Hoboken, NJ, USA: Wiley, 2021.
[4] D. A. de Arruda Mello and F. A. Barbosa, *Digital Coherent Optical Systems*. Cham, Switzerland: Springer, 2021.
[5] D. Semrau, R. I. Killey, and P. Bayvel, "A closed-form approximation of the Gaussian noise model in the presence of inter-channel stimulated Raman scattering," *J. Lightw. Technol.*, vol. 37, no. 9, pp. 1924–1936, May 1, 2019.
[6] Z. Tao, L. Dou, W. Yan, L. Li, T. Hoshida, and J. C. Rasmussen, "Multiplier-free intrachannel nonlinearity compensating algorithm operating at symbol rate," *J. Lightw. Technol.*, vol. 29, no. 17, pp. 2570–2576, Sep. 2011.
[7] P. Poggiolini, G. Bosco, A. Carena, V. Curri, Y. Jiang, and F. Forghieri, "The GN-model of fiber non-linear propagation and its applications," *J. Lightw. Technol.*, vol. 32, no. 4, pp. 694–721, Feb. 2014.
[8] M. Damzen, V. Vlad, A. Mocofanescu, and V. Babin, *Stimulated Brillouin Scattering: Fundamentals and Applications*. Boca Raton, FL, USA: CRC Press, 2003.
[9] B. Corcoran and A. Choudhary, "SBS in optical communication systems: The good, the bad and the ugly," in *Semiconductors Semimetals*, vol. 110. Cambridge, MA, USA: Academic, 2022, pp. 181–213.
[10] G. P. Agrawal, "Nonlinear fiber optics," in *Nonlinear Science at the Dawn of the 21st Century*. Berlin, Germany: Springer, 2000, pp. 195–211.
[11] S. Chandra, A. V. Vardhanan, and R. Gangopadhyay, "Simultaneous dispersion and non-linearity compensation with mid-span optical phase conjugation and distributed Raman amplifier for a sub-carrier multiplexed optical transmission link," *Opt. Commun.*, vol. 279, no. 1, pp. 177–182, Nov. 2007.
[12] A. Sobhanan, L. N. Venkatasubramani, R. D. Koilpillai, and D. Venkitesh, "Dispersion and nonlinearity distortion compensation of the QPSK/16QAM signals using optical phase conjugation in nonlinear SOAs," *IEEE Photon. J.*, vol. 12, no. 1, pp. 1–7, Feb. 2020.
[13] E. Giacoumidis, I. Aldaya, M. A. Jarajreh, A. Tsokanos, S. Thai Le, F. Farjady, Y. Jaouën, A. D. Ellis, and N. J. Doran, "Volterra-based reconfigurable nonlinear equalizer for coherent OFDM," *IEEE Photon. Technol. Lett.*, vol. 26, no. 14, pp. 1383–1386, Jul. 2014.
[14] J. Hélio C., T. Sutili, S. M. Rossi, R. C. Figueiredo, and D. A. A. Mello, "Fast adaptive digital back-propagation algorithm for unrepeatered optical systems," in *Proc. Opt. Fiber Commun. Conf. Exhib. (OFC)*, Mar. 2020, pp. 1–3.
[15] E. Ip and J. M. Kahn, "Compensation of dispersion and nonlinear impairments using digital backpropagation," *J. Lightw. Technol.*, vol. 26, no. 20, pp. 3416–3425, Oct. 2008.
[16] F. Musumeci, C. Rottondi, A. Nag, I. Macaluso, D. Zibar, M. Ruffini, and M. Tornatore, "An overview on application of machine learning techniques in optical networks," *IEEE Commun. Surveys Tuts.*, vol. 21, no. 2, pp. 1383–1408, 2nd Quart., 2019.
[17] J. Zhang, W. Chen, M. Gao, and G. Shen, "K-means-clustering-based fiber nonlinearity equalization techniques for 64-QAM coherent optical communication system," *Opt. Exp.*, vol. 25, no. 22, pp. 27570–27580, 2017.
[18] D. Zibar, O. Winther, N. Franceschi, R. Borkowski, A. Caballero, V. Arlunno, M. N. Schmidt, N. G. Gonzales, B. Mao, Y. Ye, K. J. Larsen, and I. T. Monroy, "Nonlinear impairment compensation using expectation maximization for dispersion managed and unmanaged PDM 16-QAM transmission," *Opt. Exp.*, vol. 20, no. 26, pp. B181–B196, 2012.
[19] X. Huang, Y. Wang, C. Li, H. Xu, Q. Zhang, L. Yang, and X. Xin, "Improved DBSCAN algorithm based signal recovery technology in coherent optical communication systems," *Opt. Commun.*, vol. 521, Oct. 2022, Art. no. 128590.
[20] R. A. de Paula, L. Marim, R. A. Penchel, Y. R. Bustamante, M. L. Abbade, G. Perez-Sanchez, and I. Aldaya, "Mitigation of nonlinear phase noise in single-channel coherent 16-QAM systems employing logistic regression," *Opt. Quantum Electron.*, vol. 53, p. 508, Aug. 2021.
[21] D. Wang, M. Zhang, M. Fu, Z. Cai, Z. Li, Y. Cui, and B. Luo, "KNN-based detector for coherent optical systems in presence of nonlinear phase noise," in *Proc. 21st Optoelectron. Commun. Conf. (OECC) Held Jointly Int. Conf. Photon. Switching (PS)*, Jul. 2016, pp. 1–3.
[22] D. Wang, M. Zhang, Z. Cai, Y. Cui, Z. Li, H. Han, M. Fu, and B. Luo, "Combatting nonlinear phase noise in coherent optical systems with an optimized decision processor based on machine learning," *Opt. Commun.*, vol. 369, pp. 199–208, Jun. 2016.
[23] L. M. da Silva, R. de Paula, J. A. de Oliveira, M. Santos, R. Penchel, G. G. Perez, M. L. F. Abbade, and I. Aldaya, "Nonlinear phase noise compensation in single-span digital coherent optical systems employing artificial neural networks," in *Proc. SBFoton Int. Opt. Photon. Conf. (SBFoton IOPC)*, May 2021, pp. 1–4.
[24] C. Li, Y. Wang, L. Han, S. Chen, Q. Zhang, L. Yang, and X. Xin, "Optical fiber nonlinearity equalizer with support vector regression based on perturbation theory," *Opt. Commun.*, vol. 507, Mar. 2022, Art. no. 127627.
[25] P. J. Freire, S. Srivallapanondh, M. Anderson, B. Spinnler, T. Bex, T. A. Eriksson, A. Napoli, W. Schairer, N. Costa, M. Blott, S. K. Turitsyn, and J. E. Prilepsky, "Implementing neural network-based equalizers in a coherent optical transmission system using field-programmable gate arrays," *J. Lightw. Technol.*, vol. 41, no. 12, pp. 3797–3815, Jun. 15, 2023.
[26] D. A. Ron, P. J. Freire, J. E. Prilepsky, M. Kamalian-Kopae, A. Napoli, and S. K. Turitsyn, "Experimental implementation of a neural network optical channel equalizer in restricted hardware using pruning and quantization," *Sci. Rep.*, vol. 12, no. 1, p. 8713, May 2022.
[27] M. Schaedler, C. Bluemm, M. Kuschnerov, F. Pittalà, S. Calabrò, and S. Pachnicke, "Deep neural network equalization for optical short reach communication," *Appl. Sci.*, vol. 9, no. 21, p. 4675, Nov. 2019.
[28] C. Li, Y. Wang, J. Wang, H. Yao, X. Liu, R. Gao, L. Yang, H. Xu, Q. Zhang, P. Ma, and X. Xin, "Convolutional neural network-aided DP-64 QAM coherent optical communication systems," *J. Lightw. Technol.*, vol. 40, no. 9, pp. 2880–2889, May 1, 2022.
[29] J. Ney, C. Füllner, V. Lauinger, L. Schmalen, S. Randel, and N. Wehn, "From algorithm to implementation: Enabling high-throughput CNN-based equalization on FPGA for optical communications," in *Proc. Int. Conf. Embedded Comput. Syst.* Cham, Switzerland: Springer, 2023, pp. 158–173.
[30] Y. Gong, X. Jia, Y. Zhu, K. Liu, M. Luo, J. Tao, Z. He, C. Li, Z. Liu, and Y. Li, "Complex-valued CNN nonlinear equalization enabled 36-Tbit/s (45×800-Gbit/s) WDM transmission Over 3150 Km using silicon-based IC-TROSA," *IEEE Photon. J.*, vol. 17, no. 1, Feb. 2025, Art. no. 7200108.
[31] X. Liu, Y. Wang, X. Wang, H. Xu, C. Li, and X. Xin, "Bi-directional gated recurrent unit neural network based nonlinear equalizer for coherent optical communication system," *Opt. Exp.*, vol. 29, no. 4, pp. 5923–5933, 2021.
[32] M. Schädler, G. Böcherer, F. Pittalà, S. Calabrò, N. Stojanovic, C. Bluemm, M. Kuschnerov, and S. Pachnicke, "Recurrent neural network soft-demapping for nonlinear ISI in 800Gbit/s DWDM coherent optical transmissions," *J. Lightw. Technol.*, vol. 39, no. 16, pp. 5278–5286, Aug. 15, 2021.
[33] Z. Jiang, X. Liu, and L. Zhang, "Wide and deep learning-aided nonlinear equalizer for coherent optical communication systems," *Photonics*, vol. 11, no. 2, p. 141, Feb. 2024.
[34] S. Deligiannidis, C. Mesaritakis, and A. Bogris, "Performance and complexity analysis of bi-directional recurrent neural network models versus Volterra nonlinear equalizers in digital coherent systems," *J. Lightw. Technol.*, vol. 39, no. 18, pp. 5791–5798, Sep. 2021.
[35] S. Deligiannidis, A. Bogris, C. Mesaritakis, and Y. Kopsinis, "Compensation of fiber nonlinearities in digital coherent systems leveraging long short-term memory neural networks," *J. Lightw. Technol.*, vol. 38, no. 21, pp. 5991–5999, Nov. 1, 2020.
[36] T. Koike-Akino, Y. Wang, K. Kojima, K. Parsons, and T. Yoshida, "Zero-multiplier sparse DNN equalization for fiber-optic QAM systems with probabilistic amplitude shaping," in *Proc. Eur. Conf. Opt. Commun. (ECOC)*, Sep. 2021, pp. 1–4.
[37] H. Ming, X. Chen, X. Fang, L. Zhang, C. Li, and F. Zhang, "Ultralow complexity long short-term memory network for fiber nonlinearity mitigation in coherent optical communication systems," *J. Lightw. Technol.*, vol. 40, no. 8, pp. 2427–2434, Apr. 15, 2022.
[38] X. Liu, "Enabling optical network technologies for 5G and beyond," *J. Lightw. Technol.*, vol. 40, no. 2, pp. 358–367, Jan. 15, 2022.
[39] "Selecting the right optical modulation analyzer (OMA) for manufacturing test," Quantifi Photonics, Auckland, New Zealand, Tech. Rep., Jan. 2010.
[40] S. J. Savory, "Digital coherent optical receivers: Algorithms and subsystems," *IEEE J. Sel. Topics Quantum Electron.*, vol. 16, no. 5, pp. 1164–1179, Sep. 2010.
[41] I. Goodfellow, *Deep Learning*, vol. 196. Cambridge, MA, USA: MIT Press, 2016.

[42] A. G. Reza and J. K. Rhee, "Nonlinear equalizer based on neural networks for PAM-4 signal transmission using DML," *IEEE Photon. Technol. Lett.*, vol. 30, no. 15, pp. 1416–1419, Aug. 1, 2018.
[43] M. A. Jarajreh, E. Giacoumidis, I. Aldaya, S. T. Le, A. Tsokanos, Z. Ghassemlooy, and N. J. Doran, "Artificial neural network nonlinear equalizer for coherent optical OFDM," *IEEE Photon. Technol. Lett.*, vol. 27, no. 4, pp. 387–390, Feb. 15, 2015.
[44] O. Sidelnikov, A. Redyuk, and S. Sygletos, "Equalization performance and complexity analysis of dynamic deep neural networks in long haul transmission systems," *Opt. Exp.*, vol. 26, no. 25, pp. 32765–32776, 2018.
[45] W. Freude, R. Schmogrow, B. Nebendahl, M. Winter, A. Josten, D. Hillerkuss, S. Koenig, J. Meyer, M. Dreschmann, M. Huebner, C. Koos, J. Becker, and J. Leuthold, "Quality metrics for optical signals: Eye diagram, Q-factor, OSNR, EVM and BER," in *Proc. 14th Int. Conf. Transparent Opt. Netw. (ICTON)*, Jul. 2012, pp. 1–4.
[46] S. An, Q. Zhu, J. Li, Y. Ling, and Y. Su, "112-Gb/s SSB 16-QAM signal transmission over 120-km SMF with direct detection using a MIMO-ANN nonlinear equalizer," *Opt. Exp.*, vol. 27, no. 9, pp. 12794–12805, 2019.
[47] Y. Wang, "Artificial-intelligence integrated circuits: Comparison of GPU, FPGA, and ASIC," *Appl. Comput. Eng.*, vol. 4, pp. 99–104, Jan. 2023.
[48] E. Giacoumidis, S. Mhatli, T. Nguyen, S. T. Le, I. Aldaya, M. E. McCarthy, A. D. Ellis, and B. J. Eggleton, "Comparison of DSP-based nonlinear equalizers for intra-channel nonlinearity compensation in coherent optical OFDM," *Opt. Lett.*, vol. 41, no. 11, pp. 2509–2512, 2016.
[49] K. Deb, S. Agrawal, A. Pratap, and T. Meyarivan, "A fast elitist non-dominated sorting genetic algorithm for multi-objective optimization: NSGA-II," in *Proc. Int. Conf. Parallel Problem Solving Nature*. Berlin, Germany: Springer, 2000, pp. 849–858.

LUCAS C. DANTAS received the degree in electronics and telecommunications engineering and the master's degree in electrical engineering from Unesp São João da Boa Vista Campus, in 2022 and 2025, respectively. Previously, his work experience included working with level sensors for chemical tank monitoring applications at Buckman Laboratories. He is currently an Electrical Cabin Systems Engineer with The Boeing Company.

HILDO GUILLARDI JÚNIOR received the Maintenance Electricity Certificate degree (cum laude) from the National Service for Industrial Training (SENAI), Brazil, the B.S. (cum laude) and M.Sc. degrees in electrical engineering from São Paulo State University (Unesp), Brazil, and the Ph.D. degree in electrical engineering from the University of Campinas (Unicamp), Brazil. He was a Visiting Researcher with the University of Padova, Italy. From 2012 to 2018, he held positions as a Substitute Professor with Unesp and a Trainee Professor with Unicamp. He has been an Assistant Professor with Unesp, since 2022, and a Collaborator with the Laboratory of Interdisciplinary Research in Smart Grids (LabREI), São Paulo Center for Energy Transition Studies (CPTEn), and São Paulo Center for Innovation in Public Lighting (CePIL). His current research interests include the control of power topologies, power quality, and data science.

PLINIO DESTER received the B.S. degree in engineering from École Polytechnique, France, in 2017, and the master's and Ph.D. degrees in electrical engineering from the State University of Campinas, Brazil, in 2022. He has worked in Orange Laboratories, France, the National Institute for Research in Computer Science and Automation, France, the National Center for Research in Energy and Materials, Brazil, the Federal University of Technology of Paraná, Brazil, and the State University of Campinas. He is currently an Assistant Professor of wireless communication, communication networks, and stochastic processes with São Paulo State University, Brazil. His research interests include the intersection of mathematics and telecommunications.

RAFAEL A. PENCHEL (Senior Member, IEEE) received the B.Sc. degree in telecommunications engineering from FUMEC University, Belo Horizonte, Brazil, in 2006, the M.Sc. degree in electrical engineering from the Federal University of Minas Gerais, in 2009, and the Ph.D. degree in electrical engineering from the Pontifical Catholic University of Rio de Janeiro (PUC-Rio), in 2014. In 2015, he became a Postdoctoral Fellow with the National Institute of Telecommunications (Inatel). Since 2017, he has been a Professor with the Department of Electronic and Telecommunications Engineering, São Paulo State University (Unesp) and is part of the Center for Advanced and Sustainable Technologies (CAST) Research Group. He has experience in electromagnetic theory with emphasis on microwave theory and antennas. His fields of research interest are passive devices and antennas for microwave and millimeter-wave frequencies, mainly helical antennas, microstrip patch antennas, horn and reflector antennas, beamforming networks, and 3-D-printed antennas with complex geometries via plastic and metal additive manufacturing.

JOSÉ AUGUSTO DE OLIVEIRA received the bachelor's degree in administration and a specialization in environmental management from Ceuclar, the bachelor's degree in environmental engineering from the Federal University of São Carlos (UFSCar), the master's degree in production engineering from São Paulo State University Júlio de Mesquita Filho (Unesp), and the Ph.D. degree in production engineering from the University of São Paulo (USP). He is currently a Professor with UNESP. He is the Leader of the Research Group Center for Advanced and Sustainable Technologies (CAST) and the University Extension Group Retec Unesp-Recycling Technology. He is accredited in the Graduate Program in Engineering (PPGE), School of Engineering and Sciences of Guaratinguet, Unesp, and the Graduate Program in Electrical Engineering (PGEE), School of Engineering of São João da Boa Vista and Institute of Science and Technology of Sorocaba, Unesp. Additionally, he is a member of the Network for Advances in Cleaner Production and the International Network Life Cycle Initiative (LCI), and a member of the International Network Photonics International Network (PIN), established through the CAPES PRINT UNESP International Research Networks Agreement, a Cooperation Project between Unesp, the University of Bordeaux, France, the University of Aveiro, Portugal, and Laval University, Canada. His research focuses on topics related to the EGCV of electronic and technological products, with a primary emphasis on: life cycle assessment (LCA), cleaner production (CP), ecodesign, and end-of-life (EoL) product strategies, especially recycling.

MARCELO L. F. ABBADE received the B.Sc. and M.Sc. degrees in physics, and the Ph.D. degree in electrical engineering from the University of Campinas (UNICAMP), Brazil, in 1990, 1993, and 2001, respectively. He was a Professor with the Pontifical Catholic University of Campinas, from 2002 to 2015. Since 2015, he has been with São Paulo State University (Unesp), where he was an Associate Professor with the Department of Electronics and Telecommunications. His main research interests include studying nonlinearities in optical communications and physical layer security.

LEANDRA I. ABREU received the degree in aeronautical engineering from Universidade Federal de Minas Gerais (UFMG) and the Ph.D. degree in signal processing applied to turbulent flows and aeroacoustics from Instituto Tecnológico de Aeronáutica (ITA), during which she carried out research internships at the University of Twente. She is currently an Assistant Professor with Universidade Estadual de São Paulo (Unesp) and is part of the Aerodynamics, Structural Dynamics, and Aeroelasticity Research Group. Her main research interests include signal processing, machine learning, and fluid mechanics.

JINLONG WEI (Senior Member, IEEE) received the Ph.D. degree from the University of Wales, U.K., in 2011. He is currently a Research Professor with the Peng Cheng Laboratory, Shenzhen, China. His research interests include optics communications, photonic switching/signal processing, advanced modulation/coding, digital signal processing, algorithms, and machine learning. He edited one book and (co-)authored more than 200 peer-reviewed journal/conference papers, including *Nature Electronics*, *Photonics Research*, OFC, and ECOC, and more than 20 invited. He has experimentally demonstrated a few world-first real-time and offline optical communication systems for data- and telecommunications applications, which were reported by various scientific and technical media and organizations. He holds several U.S./European patents. He is a Marie Curie fellow and a Senior Member of Optica (formerly OSA).

IVAN ALDAYA (Member, IEEE) received the degree in telecommunications engineering from the Universidad Publica de Navarra and the Ph.D. degree in information and communications technologies from the Instituto Tecnológico y de Estudios Superiores de Monterrey, during which he carried out research internships at the Università di Bologna and École Nationale Supérieure des Telecommunications. After the Ph.D., he was a Postdoctoral Researcher with the Department of Optical Communications, Instituto Tecnológico y de Estudios Superiores de Monterrey, and the Gleb Wataghin Institute of Physics, University of Campinas. He is currently an Assistant Professor with Universidade Estadual de São Paulo and is part of the Center for Advanced and Sustainable Technologies (CAST) Research Group. His main research interests include optical communications (including radio over fiber systems and digital coherent systems) and the application of artificial intelligence to optimize integrated photonic devices and antennas.

Coordenação de Aperfeiçoamento de Pessoal de Nível Superior (CAPES) - ROR identifier: 00x0ma614